JOURNAL OF COMPUTATIONAL PHYSICS 21, 371–399 (1976)

Accurate and Efficient Quadrature for Volterra Integral Equations

DWAYNE L. KNIRK

Department of Chemistry, University of California, Berkeley, California 94720

Received August 1, 1975; revised December 31, 1975

Four quadrature schemes have been tested and compared in considerable detail to determine their usefulness in the noniterative integral equation method for single channel quantum mechanical calculations. They are two forms of linear approximation (Trapezoidal rule) and two forms of quadratic approximation (Simpson's rule). Their implementation in this method is shown, a formal discussion of error propagation is given, and tests are performed to determine actual operating characteristics on various bound and scattering problems in different potentials. The quadratic schemes are generally superior to the linear ones in terms of accuracy and efficiency. The previous implementation of Simpson's rule is shown to possess an inherent instability which requires testing on each problem for which it is used to assure its reliability. The alternative quadratic approximation which we propose does not suffer this deficiency, but still enjoys the advantages of higher order. In addition, the new scheme obeys very well an h^4 Richardson extrapolation, whereas the old one does so rather poorly.

1. INTRODUCTION

In recent years, the noniterative integral equation method suggested by Sams and Kouri [1] for close-coupled calculations has been applied successfully several times to both scattering and bound state problems [2]. While some work has been done toward investigating various quadrature schemes [3], we have undertaken a more extensive study of four different schemes aimed at recommending a "best available" scheme for the noniterative method. We make comparisons based on efficiency considerations and error characteristics for each scheme.

We expect efficiency considerations to be meaningful here—the same programming skills will be used with each scheme since there is only one programmer. Storage requirements for the various schemes have not been analyzed in detail. We have attempted to analyze error propagations analytically, and have then examined actual errors in numerous computations. Finally, a generalization of the Richardson extrapolation technique has been proposed and shown to be very useful for obtaining highly accurate results.

This paper presents results on single channel calculations only. The corresponding multichannel study is now in progress, and both efficiency and storage are of importance there.

2. The Problem and Its Special Properties

We are interested in the numerical solution ψ of the equation

$$\psi(r) = u(r) + \int_0^\infty f(r_<)\, g(r_>)\, V(r')\, \psi(r')\, dr', \tag{1}$$

where u, f, g, and V are known functions. The extension of our techniques to coupled equations, or even those containing finite rank nonlocal potentials is straightforward. We shall apply (1) to the calculation of both scattering states ($u = f$) and bound states ($u = 0$).

For either u, (1) may be put into the equivalent Volterra form (see Appendix A)

$$\phi(r) = g(r)\, A(r) + f(r)\, B(r), \tag{2a}$$

$$A(r) = \int_0^r f(r')\, V(r')\, \phi(r')\, dr', \tag{2b}$$

$$B(r) = 1 - \int_0^r g(r')\, V(r')\, \phi(r')\, dr', \tag{2c}$$

where $\phi(r)$ is some multiple of ψ. These are the basic equations of the noniterative method. To examine their properties, it is convenient to define the vector

$$\mathbf{P}(r) = \begin{pmatrix} A(r) \\ B(r) \end{pmatrix}. \tag{3}$$

By differentiating (2b) and (2c), and using (2a), one easily obtains the coupled, first-order differential equations [4]

$$\mathbf{P}'(r) = \mathbf{M}(r) \cdot \mathbf{P}(r), \qquad \mathbf{P}(0) = \begin{pmatrix} 0 \\ 1 \end{pmatrix}, \tag{4}$$

where

$$\mathbf{M}(r) = \begin{pmatrix} fVg & fVf \\ -gVg & -gVf \end{pmatrix}. \tag{5}$$

These equations are completely equivalent to (2), and permit a wide range of methods of solution [5, 6].

The martrix **M** has two important properties. First, it can be expressed as the outer product of two vectors,

$$\mathbf{U}(r) = \begin{pmatrix} g(r) \\ f(r) \end{pmatrix}, \qquad \mathbf{W}(r) = \begin{pmatrix} f(r) \\ -g(r) \end{pmatrix} \tag{6}$$

by

$$\mathbf{M}(r) = \mathbf{W}(r)\, V(r)\, \mathbf{U}^{\dagger}(r). \tag{7}$$

Furthermore, since **U** and **W** are orthogonal, **M** is nilpotent and

$$\mathbf{M}(r) \cdot \mathbf{P}'(r) = \mathbf{0}. \tag{8}$$

This second property gives the method its noniterative character, as we now demonstrate. The schemes we consider here for integrating (4) are based on numerical integration formulas of the general form [7]

$$\mathbf{P}_n = \mathbf{P}_m + \sum_{j=m}^{n} \alpha_j \mathbf{P}_j', \tag{9}$$

where $\{\alpha_j\}$ are a set of quadrature weights, $\mathbf{P}_j = \mathbf{P}(r_j)$, and $\{r_j\}$ are the quadrature points. If we multiply (9) by $\mathbf{M}_n$ and use (4) and (8), we obtain

$$\mathbf{P}_n' = \mathbf{M}_n \cdot \left(\mathbf{P}_m + \sum_{m}^{n-1} \alpha_j \mathbf{P}_j' \right). \tag{10}$$

This is then used to eliminate $\mathbf{P}_n'$ from the r.h.s. of (9), with the result

$$\mathbf{P}_n = (\mathbf{1} + \alpha_n \mathbf{M}_n) \cdot \left(\mathbf{P}_m + \sum_{m}^{n-1} \alpha_j \mathbf{P}_j' \right). \tag{11}$$

Thus, **P** at r_n only depends on **P** at earlier quadrature points. Because one can obtain $\mathbf{P}_n'$ before obtaining $\mathbf{P}_n$, closed-form integration formulas with their attendant high accuracy may be employed *without* the usual predictor–corrector type iteration.

This demonstration can also be given in the usual wavefunction form by noting that

$$\phi_j = \mathbf{U}_j^{\dagger} \cdot \mathbf{P}_j. \tag{12}$$

Using (4), (7), and (12) in (9) and setting $m = 0$ gives the quadrature form of (2a)

$$\phi_n = f_n + \mathbf{U}_n^{\dagger} \cdot \sum_{0}^{n-1} \alpha_j \mathbf{W}_j V_j \phi_j ; \tag{13}$$

the term $j = n$ vanishes by orthogonality of $\mathbf{U}_n$ and $\mathbf{W}_n$. For the numerical analysis of the noniterative method, we think $\mathbf{P}$ to be the proper object of attention; derivations are much more concise, and the method of error analysis is more apparent. As a bonus, the algorithms we have constructed from these derivations are slightly more efficient than what we were able to construct from the wave-function derivations of the same quadrature schemes.

3. Quadrature Schemes

The four schemes considered in this paper for the integration of (4) are (A) the trapezoidal rule, (B) the "overlapped" trapezoidal rule, (C) our own quadratic rule, and (D) the "overlapped" Simpson's rule. We have coded reasonably efficient algorithms for each scheme, and indicate the investment per step of solution by giving the number of multiplications required (the number of additions being insignificant).

(A) *Trapezoidal Rule*

This is the most-used scheme of the four. The rule is

$$\mathbf{P}_{n+1} = \mathbf{P}_n + (h/2)(\mathbf{P}_n' + \mathbf{P}'_{n+1}), \tag{14}$$

where h is the step size, and the local truncation error is $-h^3P'''/12$. Following (9)–(11), we obtain the working equation

$$\mathbf{P}_{n+1} = (\mathbf{1} + (h/2)\,\mathbf{M}_{n+1}) \cdot (\mathbf{P}_n + (h/2)\,\mathbf{P}_n'). \tag{15}$$

This is most efficiently programmed by defiining the auxillary vector

$$\mathbf{Q}_n = \mathbf{P}_n + (h/2)\,\mathbf{P}_n' = (\mathbf{1} + (h/2)\,\mathbf{M}_n) \cdot \mathbf{P}_n \tag{16}$$

and doing all integrations, except the first and last step, by

$$\mathbf{Q}_{n+1} = (\mathbf{1} + h\mathbf{M}_{n+1}) \cdot \mathbf{Q}_n\,. \tag{17}$$

Integration by this scheme requires six multiplications to advance from r_n to r_{n+1}.

(B) *Overlapped Trapezoidal Rule*

For ordinary first-order equations, Milne suggests the simple midpoint rule [8]

$$\mathbf{P}_{n+2} = \mathbf{P}_n + 2h\mathbf{P}'_{n+1} = \mathbf{P}_n + 2h\mathbf{M}_{n+1} \cdot \mathbf{P}_{n+1}\,, \tag{18}$$

where h is again the step size, and the local truncation error is $h^3P'''/3$. Given $\mathbf{P}$ at r_n and r_{n+1}, this allows its evaluation at r_{n+2}. The scheme continues by "overlapping" the rule at points r_{n+1} and r_{n+2} to get $\mathbf{P}$ at r_{n+3}. Since only $\mathbf{P}_0$ is given, some other scheme such as scheme (A) must be used to obtain a $\mathbf{P}_1$ in order to start this procedure. This scheme also requires six multiplications per step.

(C) *Quadratic Rule*

This scheme is new, and is one of the main results of this paper [9]. It uses Simpson's rule (a quadratic approximation) in both the one- and two-step forms [10]

$$\mathbf{P}_{n+1} = \mathbf{P}_n + (h/12)(5\mathbf{P}_n' + 8\mathbf{P}'_{n+1} - \mathbf{P}'_{n+2}), \tag{19}$$

$$\mathbf{P}_{n+2} = \mathbf{P}_n + (h/3)(\mathbf{P}_n' + 4\mathbf{P}'_{n+1} + \mathbf{P}'_{n+2}). \tag{20}$$

These rules have local truncation errors of $h^4\mathbf{P}^{(4)}/24$ and $-h^5\mathbf{P}^{(5)}/90$, respectively. respectively. We multiply (19) by $\mathbf{M}_{n+1}$ to get an equation for $\mathbf{P}'_{n+1}$ in terms of $\mathbf{P}'_{n+2}$, and multiply (20) by $\mathbf{M}_{n+2}$ to get an equation for $\mathbf{P}'_{n+2}$ in terms of $\mathbf{P}'_{n+1}$. These can be solved by simple substitution to get

$$\mathbf{L}_1 \cdot \mathbf{P}'_{n+1} = \mathbf{M}_{n+1} \cdot (\mathbf{R}_n - (h/12)\,\mathbf{M}_{n+2} \cdot \mathbf{S}_n), \tag{21}$$

$$\mathbf{L}_2 \cdot \mathbf{P}'_{n+2} = \mathbf{M}_{n+2} \cdot (\mathbf{S}_n + (4h/3)\,\mathbf{M}_{n+1} \cdot \mathbf{R}_n), \tag{22}$$

where

$$\mathbf{L}_1 = \mathbf{1} + (h^2/9)\,\mathbf{M}_{n+1} \cdot \mathbf{M}_{n+2}, \tag{23}$$

$$\mathbf{L}_2 = \mathbf{1} + (h^2/9)\,\mathbf{M}_{n+2} \cdot \mathbf{M}_{n+1}, \tag{24}$$

$$\mathbf{R}_n = \mathbf{P}_n + (5h/12)\,\mathbf{P}_n', \tag{25}$$

$$\mathbf{S}_n = \mathbf{P}_n + (h/3)\,\mathbf{P}_n'. \tag{26}$$

The special properties of $\mathbf{M}$ now allow immediate inversion of $\mathbf{L}_1$ and $\mathbf{L}_2$. In fact, these matrices are easily shown to be multiples of each others' inverses:

$$\mathbf{I}p^{-1} = \mathbf{L}_1 \cdot \mathbf{L}_2 = \mathbf{L}_2 \cdot \mathbf{L}_1 = [1 - (\tfrac{1}{3}\,eh)^2\,V_{n+1}V_{n+2}]\,\mathbf{I}, \tag{27}$$

$$e = \mathbf{U}^{\dagger}_{n+2} \cdot \mathbf{W}_{n+1} = g_{n+2}f_{n+1} - f_{n+2}g_{n+1}. \tag{28}$$

Therefore, multiplying (21) by $\mathbf{L}_2$, and noting $\mathbf{L}_2 \cdot \mathbf{M}_{n+1} = \mathbf{M}_{n+1}$, gives

$$\mathbf{P}'_{n+1} = p\mathbf{M}_{n+1} \cdot (\mathbf{R}_n - (h/12)\,\mathbf{M}_{n+2} \cdot \mathbf{S}_n), \tag{29}$$

and multiplying (22) by $\mathbf{L}_1$, noting $\mathbf{L}_1 \cdot \mathbf{M}_{n+2} = \mathbf{M}_{n+2}$, gives

$$\mathbf{P}'_{n+2} = p\mathbf{M}_{n+2} \cdot (\mathbf{S}_n + (4h/3)\,\mathbf{M}_{n+1} \cdot \mathbf{R}_n). \tag{30}$$

These two results are then used in (20) to get $\mathbf{P}_{n+2}$. We keep both $\mathbf{P}_n$ and $\mathbf{P}_n'$ in storage to advance from r_n to r_{n+2}. We then keep $\mathbf{P}_{n+2}$ and $\mathbf{P}'_{n+2}$ for the next cycle. By calculating and storing combinations of constants beforehand (note that e is independent of n for fixed h) we have constructed an algorithm requiring 26 multiplications and 13 additions, or 13 multiplications *per step*.

Because the result is useful later for deriving the error law, we note that (19) can be multiplied by $(4h/3)\,\mathbf{M}_{n+1}$ and added to (20) to give an equation relating $\mathbf{P}_{n+2}$ and $\mathbf{P}_n$ directly:

$$\left(\mathbf{1} - \frac{h}{3}\mathbf{M}_{n+2} + \frac{h^2}{9}\mathbf{M}_{n+1} \cdot \mathbf{M}_{n+2}\right) \cdot \mathbf{P}_{n+2}$$

$$= \left(\mathbf{1} + \frac{h}{3}\mathbf{M}_n + \frac{4h}{3}\mathbf{M}_{n+1} + \frac{h^2}{9}\mathbf{M}_{n+1} \cdot \mathbf{M}_n\right) \cdot \mathbf{P}_n\,. \tag{31}$$

The necessity of inverting the matrix on the l.h.s. makes this procedure far more difficult than the one we have given.

(D) *Overlapped Simpson's Rule*

Finally, we consider the application of Simpson's rule which has been made previously [3]. Employing the transformations (9)–(11) on the rule in (20), we get

$$\mathbf{P}_{n+2} = (\mathbf{1} + (h/3)\,\mathbf{M}_{n+2}) \cdot (\mathbf{P}_n + (h/3)\,\mathbf{P}_n' + (4h/3)\,\mathbf{P}'_{n+1}). \tag{32}$$

Given $\mathbf{P}$ at r_n and r_{n+1}, we get $\mathbf{P}_{n+2}$ with a local truncation error $-h^5\mathbf{P}^{(5)}/90$. "Overlapping" the rule at r_{n+1} and r_{n+2} then gives $\mathbf{P}_{n+3}$, and so on. As with scheme (B), only $\mathbf{P}_0$ is given, so another scheme (such as scheme (A)) must be used to start this procedure. The algorithm here requires 11 multiplications per step. Note that two vectors, $\mathbf{P}_n$ and $\mathbf{P}_n'$, need to be stored for each step.

4. Formal Error Analysis

We have analyzed theoretically the effects of truncation and propagation of errors for each quadrature scheme, following the approach in standard reference texts [6–11]. Denoting the exact solution of (4) by $\bar{\mathbf{P}}$, the error at step n is the vector

$$\boldsymbol{\epsilon}_n = \mathbf{P}_n - \bar{\mathbf{P}}_n\,. \tag{33}$$

Also, due to the linearity of (4), the error in derivatives is simply

$$\epsilon_n' \equiv \mathbf{P}_n' - \bar{\mathbf{P}}_n' = \mathbf{M}_n \cdot \epsilon_n . \tag{34}$$

By "exact solution," we mean that $\bar{\mathbf{P}}$ satisfies the quadrature formula with the truncation term included; e.g., for scheme (A)

$$\bar{\mathbf{P}}_{n+1} = (\mathbf{1} + (h/2)\,\mathbf{M}_{n+1}) \cdot (\bar{\mathbf{P}}_n + (h/2)\,\bar{\mathbf{P}}_n') + \mathbf{T}_{n+1} . \tag{35}$$

To obtain formulas for the errors ϵ_n, we use the standard assumptions that over a range of steps, Nh, both $\mathbf{M}$ and $\mathbf{T}$ are approximately constant. Taking $\mathbf{M}$ locally constant brings about considerable simplification of the formulas due to its nilpotency. The error equations deduced then from (15), (18), (31), and (32) are

$$\text{(A)} \qquad \epsilon_{n+1} = (\mathbf{1} + h\mathbf{M}) \cdot \epsilon_n - \mathbf{T}_A , \tag{36a}$$

$$\text{(B)} \qquad \epsilon_{n+2} = 2h\mathbf{M} \cdot \epsilon_{n+1} + \epsilon_n - \mathbf{T}_B , \tag{36b}$$

$$\text{(C)} \qquad \epsilon_{n+2} = (\mathbf{1} + 2h\mathbf{M}) \cdot \epsilon_n - \mathbf{T}_C , \tag{36c}$$

$$\text{(D)} \qquad \epsilon_{n+2} = (4h/3)\,\mathbf{M} \cdot \epsilon_{n+1} + (\mathbf{1} + (2h/3)\,\mathbf{M}) \cdot \epsilon_n - \mathbf{T}_D , \tag{36d}$$

where $\mathbf{T}_A$ and $\mathbf{T}_B$ are proportional to h^3, the other two to h^5. Before analyzing these difference equations, we point out that they group themselves into two distinct classes; (A) and (C) are structurally equivalent, as are (B) and (D). The numerical results obtained later confirm this dichotomy.

An understanding of sorts may be obtained by ignoring the coupled nature of (36) and replacing the off-diagonal elements of $\mathbf{M}$ by zero. This examines the way errors in $A(r)$ depend on A, and errors in $B(r)$ depend on B. We let

$$\eta = \pm h(fVg) \tag{37}$$

with the $+$ $(-)$ sign taken for errors in A (B). For schemes (A) and (C), the results follow immediately [12]:

$$\epsilon_n = \lambda^n \epsilon_0 + \tau, \tag{38}$$

$$\text{(A)} \qquad \lambda = 1 + \eta, \qquad \tau = T/\eta,$$

$$\text{(C)} \qquad \lambda = (1 + 2\eta)^{1/2}, \qquad \tau = T/2\eta,$$

where ϵ_0 is an arbitrary constant. In either case, λ is either > 1 or < 1 as η is > 0 or < 0. Thus, the error grows or decays steadily. On the other hand, for (B) and (D), we follow Milne [13] to obtain

$$\epsilon_n = \lambda^n \epsilon_{0\lambda} + (-\mu)^n\, \epsilon_{0\mu} + T/2\eta, \tag{39}$$

$$\text{(B)} \qquad \lambda = \eta + (1 + \eta^2)^{1/2}, \qquad \mu = -\eta + (1 + \eta^2)^{1/2},$$

$$\text{(D)} \qquad \lambda = \tfrac{2}{3}\eta + (1 + \tfrac{2}{3}\eta + \tfrac{4}{9}\eta^2)^{1/2}, \qquad \mu = -\tfrac{2}{3}\eta + (1 + \tfrac{2}{3}\eta + \tfrac{4}{9}\eta^2)^{1/2},$$

where $\epsilon_{0\lambda}$ and $\epsilon_{0\mu}$ are arbitrary. When η is small, either $\lambda > 1$ for $\eta > 0$, or $\mu > 1$ for $\eta < 0$. Accordingly, the error always grows, and may alternate in sign as well. Note that these behaviors are essentially independent of the order of truncation.

Of the several approaches tried for analyzing the full error laws, all but one were frustrated by the extreme degeneracy of **M**. This degeneracy is exemplified by the remark that **M** turns any vector parallel to **W**, except **W** itself, which it annihilates. We take advantage of this to triangularize the error laws. Specifically, let

$$\boldsymbol{\epsilon}_n = a_n \mathbf{U} + b_n \mathbf{W}, \tag{40}$$

$$\mathbf{T} = \alpha \mathbf{U} + \beta \mathbf{W}. \tag{41}$$

In all cases we take $\boldsymbol{\epsilon}_0 = 0$, and for (B) and (D) we also take $\boldsymbol{\epsilon}_1 = 0$. As described above, the action of **M** on any vector $\boldsymbol{\epsilon}_m$ is

$$h\mathbf{M} \cdot \boldsymbol{\epsilon}_m = \gamma a_m \mathbf{W}, \tag{42}$$

$$\gamma = hV\mathbf{U}^{\dagger} \cdot \mathbf{U}. \tag{43}$$

Substituting (40) and (41) into (36), and using (42), we can equate separately the coefficients of **U** and of **W**. We find the equations for a_n are uncoupled from those of b_n and are easily solved. For example, for (A),

$$a_{n+1} = a_n - \alpha, \qquad a_n = -n\alpha;$$

similar results obtain for the other cases. The equations for b_n, with the explicit form of a_n inserted, then lead to essentially the same law for all cases: b_n is proportional to $n\beta$ and $n^2\gamma\alpha$.

We do not go into more detail here because the results do not describe the numerical experiments in the next section. This is due to the assumed constancy of **M** over the range r to $r + Nh$. In practice, we are interested in taking as large a step size as possible, and the range of h we investigate renders both the assumed constancy of **M** and the subsequent analysis invalid.

It is interesting that the crude analysis in (38) and (39) actually describes the results of the numerical experiments. Also, based upon the explicit form of **M** in regions of interest, certain approximations may be introduced into the full laws, and the altered coupled laws do show behavior similar to (38) and (39). However, since the assumptions on which these results are based are hard to really justify, we do not pursue this here.

A heuristic explanation of the distinct behaviors of schemes (C) and (D) hinges on the nilpotency of **M**. In (D), $\mathbf{P}_{n+2}$ only depends on the *derivative* of $\mathbf{P}_{n+1}$. This derivative tells $\mathbf{P}_{n+2}$ nothing about $\mathbf{P}_{n+1}$ itself, since $\mathbf{M}_{n+1}^{-1}$ does not exist. Thus, the abscissas at even and odd quadrature points are quite independent. On the other

hand, in (C), the simultaneous solution for $\mathbf{P}'_{n+1}$ and $\mathbf{P}'_{n+2}$ using (19) and (20) actually implies that $\mathbf{P}_{n+1}$ and $\mathbf{P}_{n+2}$ must lie on the same segment of parabola issuing from $\mathbf{P}_n$. This forces a continuity onto $\mathbf{P}_n$, $\mathbf{P}_{n+1}$, and $\mathbf{P}_{n+2}$ which does not allow significant oscillations to develop.

5. Numerical Experiments and Comparison of Schemes

We have coded all four quadrature schemes in standard FORTRAN and applied them to the calculation of both bound and scattering states in several potentials. A handy criterion of comparison is the "efficiency index" θ_s, defined as follows. Specify a tolerance of error to be allowed in the calculated result. This will require h for scheme s to be less than some maximum step h_s. Of course, h_s also depends on the problem. Then, for a scheme which requires n_s operations per step, we define

$$\theta_s \equiv h_s/n_s . \tag{44}$$

The interpretation of θ_s follows from noting that L/θ_s is the total number of operations for scheme s to integrate a distance L, keeping the error of the calculated result within the specified tolerance. Generally, the larger θ_s, the more efficient is the scheme (storage considerations excepted).

We remark that we have been assuming the functions f, g, and V to be given. In practice, a significant portion of the total computation time is devoted to their evaluation, especially in large multichannel calculations. Thus, θ_s is a quite conservative measure: Methods having larger h_s (fewer evaluations of f, g, and V) may be *much* more efficient overall than θ_s would suggest. In the numerical experiments, we shall find the following rules: (1) θ_A and θ_B are always smaller than θ_C and θ_D, although often on the same order of magnitude; (2) the quadratic schemes have h_s values roughly four times as large as those for the linear schemes. We shall also find scheme (B) is not a useful computational alternative, but it has been treated on an equal basis with the others, inasmuch as it bears the same relationship to (A) within the linear approximation as (D) does to (C) within the quadratic approximation.

Eigenvalues E of bound state problems ($E < 0$) are found by using

$$f(r) = \kappa^{-1/2} \sinh \kappa r, \qquad g(r) = -\kappa^{-1/2} e^{-\kappa r} \tag{45}$$

and adjusting E ($= -\frac{1}{2}\kappa^2$) until $B(r)$ vanishes for large r. For scattering problems ($E > 0$),

$$f(r) = k^{-1/2} \sin kr, \qquad g(r) = -k^{-1/2} \cos kr, \tag{46}$$

where $k = (2E)^{1/2}$ and the quantity of interest is the phase shift δ, defined by $\tan \delta = \lim_{r\to\infty} [-A(r)/B(r)]$. For simplicity, we have used only the $l = 0$ Green functions here. Throughout this paper we have avoided a factor of 2 appearing with V by assuming the units of V are those of $2E$ (i.e., for E in a.u., V is in Ryd.). The zero of energy is fixed by $\lim_{r\to\infty} V(r) = 0$. Finally, note that for these choices of f and g, the wavefunction ϕ has the normalization $d\phi(0)/dr = k^{1/2}$ or $\kappa^{1/2}$.

In the following problems, we examine errors in the bound state E and scattering state δ values calculated by each scheme. Such calculated quantities are functions of h and depend upon the scheme used for their evaluation; they will be denoted generically by $q_s(h)$. We distinguish errors in q_s from the error ϵ_n discussed in the last section, but shall consider both kinds. This corresponds to the usual distinction between "goodness" of expectation values of wavefunctions and "goodness" of the wavefunctions themselves.

The problem we have analyzed in greatest detail was chosen because analytical results are available for $A(r)$, $B(r)$, the eigenvalues and the phase shifts. Thus errors in the schemes can readily be assessed exactly and a fairly rigorous comparison of schemes made. The potential is the square well

$$\begin{aligned} V &= -8, \quad 0 \leqslant r \leqslant 2, \\ &= \ 0, \quad 2 < r. \end{aligned} \tag{47}$$

TABLE I

First Eigenvalue $E^{(1)}$ of the Square Well, Calculated by Each Scheme for Several Step Sizes[a]

h	(A)	(B)	(C)	(D)
0.2	−3.213172462	−10.147923140	−3.118603298	−4.094478625
0.1	−3.142751128	−4.923566462	−3.119867575	−3.274408525
0.05	−3.125620651	−3.432174197	−3.119946357	−3.141154734
0.025	−3.121366952	−3.162303213	−3.119951278	−3.122723994
0.0125	−3.120305323	−3.125096751	−3.119951586	−3.120306119
0.00625	−3.120040028	−3.120517178	−3.119951607	−3.119996432
0*	−3.119951447	−3.112694597	−3.119951607	−3.120144927
0+	−3.119949052	−3.072346218	−3.119951606	−3.121495278
		Exact −3.119951606		

[a] Row 0* contains results extrapolated from $h = 0.0125$; row 0+ contains those extrapolated from $h = 0.025$.

TABLE II

Second Eigenvalue $E^{(2)}$ of the Square Well, Calculated by Each Scheme for Several Step Sizes[a]

h	(A)	(B)	(C)	(D)
0.2	−0.759086556	−10.14792314	−0.712399450	−0.419183796
0.1	−0.710351664	−4.923566461	−0.695711285	−0.650260895
0.05	−0.698566183	−0.522190408	−0.694735794	−0.688844991
0.025	−0.695643760	−0.668994982	−0.694675718	−0.693935629
0.0125	−0.694914636	−0.691126611	−0.694671976	−0.694579356
0.00625	−0.694732446	−0.694164345	−0.694671742	−0.694660157
0*	−0.694671595	−0.698503821	−0.694671727	−0.694622271
0+	−0.694669619	−0.717929840	−0.694671713	−0.694275005
		Exact −0.694671728		

[a] Row 0* contains results extrapolated from $h = 0.0125$; row 0+ contains those extrapolated from $h = 0.025$.

TABLE III

Square Well Phase Shift for $E = 1$, Calculated by Each Scheme for Several Step Sizes[a]

h	(A)	(B)	(C)	(D)
0.2	0.365652838	1.094357722	0.342331962	0.295750148
0.1	0.339598001	0.343282890	0.332317936	0.329027631
0.05	0.333623353	0.303820559	0.331715076	0.331420666
0.025	0.332160255	0.327853104	0.331677696	0.331647462
0.0125	0.331796345	0.331079066	0.331675363	0.331671976
0*	0.331675042	0.332154387	0.331675207	0.331673610
0+	0.331672556	0.335863952	0.331675204	0.331662582
		Exact 0.331675210		

[a] Row 0* contains results extrapolated from $h = 0.0125$; row 0+ contains those extrapolated from $h = 0.025$.

TABLE IV

Square Well Phase Shift for $E = 10$, Calculated by Each Scheme for Several Step Sizes[a]

h	(A)	(B)	(C)	(D)
0.2	−1.498007285	−1.684422131	−1.530819741	−1.540923503
0.1	−1.551577940	−1.587401988	−1.565583771	−1.562664423
0.05	−1.564056012	−1.574156911	−1.56795650	−1.567422906
0.025	−1.567122343	−1.569884707	−1.568129477	−1.568049857
0.0125	−1.567885661	−1.568610640	−1.568139164	−1.568128588
0*	−1.568140100	−1.568185951	−1.568139810	−1.568133837
0+	−1.568144453	−1.568460639	−1.568139732	−1.568091654
		Exact −1.568139814		

[a] Row 0* contains results extrapolated from $h = 0.0125$; row 0+ contains those extrapolated from $h = 0.025$.

We calculated the two lowest eigenvalues $E^{(1)}$ and $E^{(2)}$ (converged to nine significant figures) and phase shifts $\delta^{(1)}$ and $\delta^{(2)}$ for two energies by all four schemes and with several step sizes. The results are shown in Tables I–IV, along with the exact values (see Appendix B). It is evident that the calculated quantities approach the exact ones quite closely as h gets small enough, regardless of which integration scheme is employed. It is more useful, though, to inquire how good the calculated results are as h gets larger. To examine this, consider the percentage errors $p_s(h)$, in the calculated quantities. These are graphed as functions of h on log–log scales in Figs. 1–4. From these figures it is easy to obtain h_s, and hence θ_s. We select the reasonable tolerance of 0.1% and read off the required h_s values. These and the computed θ_s are listed in Table V. We conclude that for bound states, schemes (A) and (C) are superior ($\theta_C > \theta_A > \theta_D > \theta_B$) while for scattering states (C) and (D) are to be preferred ($\theta_C > \theta_D > \theta_A > \theta_B$). We also note that h_C is three to seven times larger than h_D for bound states, and nearly $4h_D/3$ for both scattering states.

Returning to the percentage errors, we note that for $0.025 < h < 0.1$, the p_s values span several orders of magnitude, with the orderings

$$p_C < p_A < p_D < p_B \qquad \text{for } E > 0,$$

$$p_C < p_D < p_A < p_B \qquad \text{for } E > 0.$$

However, it appears from the figures that these orderings will change for different values of h. In particular, Figs. 3 and 4 suggest that for $h \sim 0.4$, both p_C and p_D

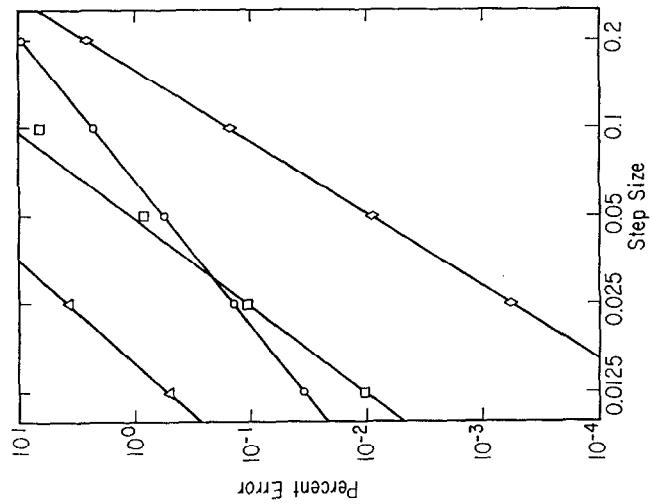

FIG. 2. Percent error in $E^{(2)}$ for the square well. See Fig. 1 for legend.

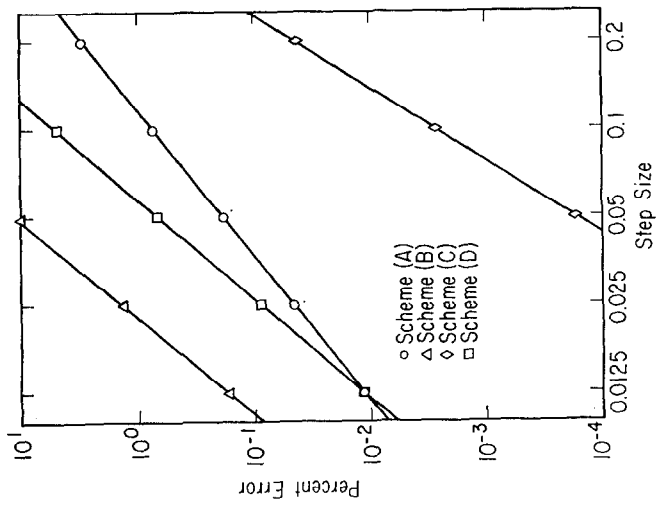

FIG. 1. Percent error in $E^{(1)}$ for the square well.

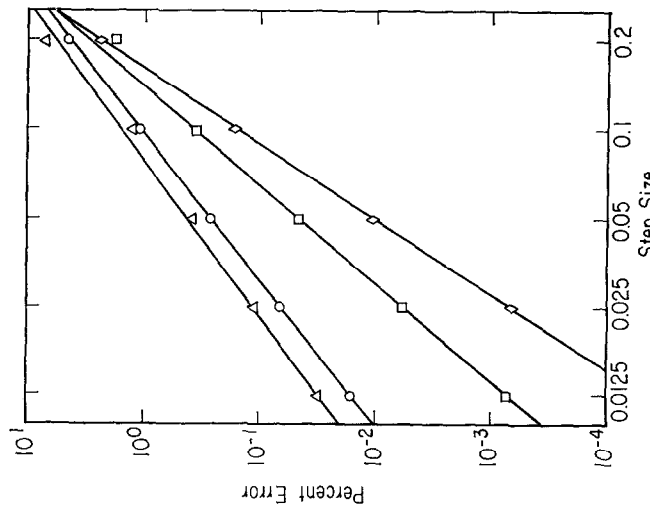

FIG. 4. Percent error in $\delta^{(2)}$ for the square well. See Fig. 1 for legend.

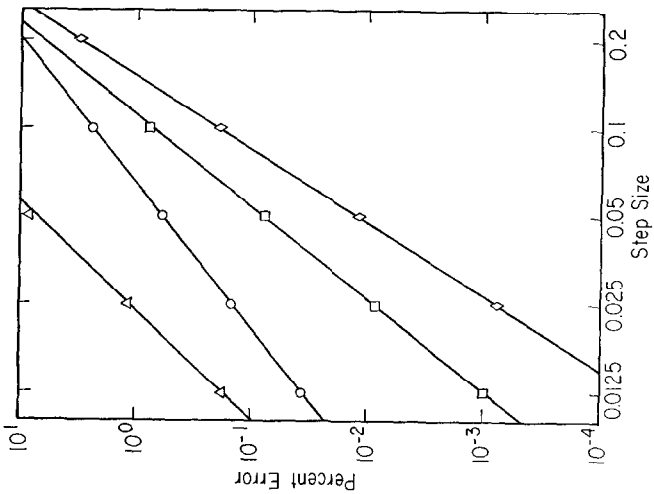

FIG. 3. Percent error in $\delta^{(1)}$ for the square well. See Fig. 1 for legend.

TABLE V

Summary of Efficiency Parameters from the Calculations on the Square Well

		(A)	(B)	(C)	(D)
$E^{(1)}$	h_s	0.037	0.005	0.247	0.032
	$10^3\theta_s$	6.18	0.78	19.0	2.87
$E^{(2)}$	h_s	0.021	0.003	0.082	0.030
	$10^3\theta_s$	3.52	0.50	6.31	2.72
$\delta^{(1)}$	h_s	0.021	0.005	0.085	0.054
	$10^3\theta_s$	3.44	0.85	6.53	4.92
$\delta^{(2)}$	h_s	0.031	0.026	0.088	0.062
	$10^3\theta_s$	5.16	4.37	6.76	5.62

will exceed p_A. This change in the ordering of p_A and p_D was noted by Hayes and Kouri [3].

Around $h = 0.05$, the large range in p_s for different s is impressive. Specifically, we have $p_B \gg p_A$ and $p_D \gg p_C$. This might be unexpected since both (A) and (B) have similar local truncation errors, as do both (C) and (D). The reason for such discrepancy is related to the error propagation characteristics of the schemes. This connection is obvious when one recalls that both eigenvalues and phase shifts are determined directly from the values of $A(2)$ and $B(2)$, so the question is how quadrature errors get into these values. We have examined this by comparing the calculated functions $B_s(r)$ with the exact $B(r)$ in Appendix B for both a negative and a positive energy.

For $E = -3$, the exact $B(r)$ is a monotone decreasing function between $B(0) = 1$ and $B(2) = -0.0031$. In Figs. 5a and 5b we show the *deviations* of the calculated $B_s(r)$ from this exact one. Note that the deviations for scheme (B) have been scaled down by a factor of 1/10 to get them in the figure. We note a curious distinction in the errors at even and odd quadrature points for the early steps of (C). As pointed out in its derivation, (C) only needs to calculate $A(r)$ and $B(r)$ at even points. Four additional statements were added to the routine to get the values at odd points also. We believe this distinction in errors in the first eight steps is due to the different orders of the local truncation in (19) and (20). The errors in both (A) and (C) appear to be damped, so this effect soon disappears. For both (B) and (D), the errors at consecutive quadrature points are seen to oscillate with growing magnitude. In the figure, the even and odd sets of points have been connected and are noted to always lie on opposite sides of zero.

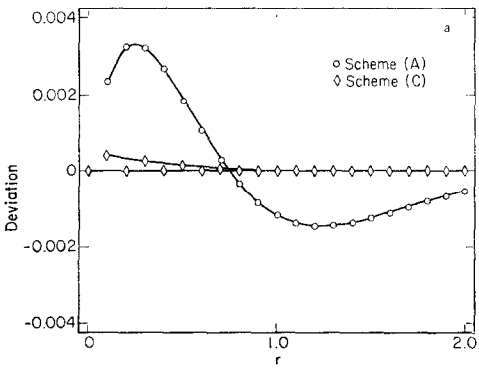

FIG. 5a. Deviations in $B(r)$ from the exact function for $E = -3$.

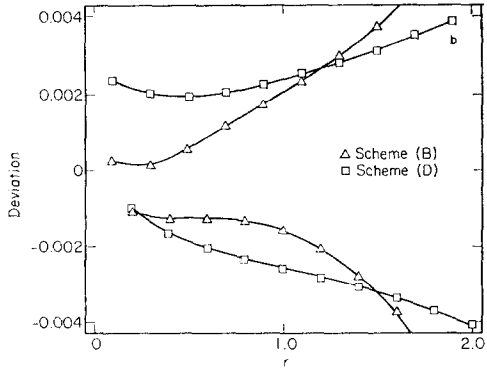

FIG. 5b. Deviations in $B(r)$ from the exact function for $E = -3$. Those for scheme (B) are 10 times larger than indicated.

The results in Fig. 5 correspond very closely to the behavior suggested by the "crude" error analysis in the last section. The parameter η for these calculations of $B(r)$ is

$$\eta = -8h\kappa^{-1} \sinh \kappa r e^{-\kappa r} < 0. \tag{48}$$

Thus, (38) and (39) show that errors in (A) and (C) should be damped, while those in (B) and (D) should oscillate and grow.

For $E = 1$, the exact $B(r)$ is again a monotone decreasing function between $B(0) = 1$ and $B(2) = -0.9448$. Deviations of the calculated $B_s(r)$ from this function are shown in Figs. 6a and 6b. Errors in (C) again bifurcate, but this time they remain distinct; the even and odd points show an interesting intertwined sinusoidal behavior. On the other hand, errors in (A) veer sharply away from zero to a maximum deviation of 0.0106 at $r = 1.5$, then return as abruptly toward zero. For (B) and (D), the deviations oscillate and grow to some maximum values between $r = 1.0$ and 1.3, then turn around and invert through zero. Note that errors in (B) had to be scaled by a factor of 1/10 again to get them on the figure.

As for the negative energy case, these errors are nicely described by the "crude" error analysis. This time,

$$\eta = -4hk^{-1} \sin 2kr. \tag{49}$$

The wavelength $2\pi/k$ for an energy $E = 1$ is $\lambda = 4.4$. This gives η a wavelength of 2.2, which means

$$\eta < 0, \qquad 0 \leqslant r \leqslant 1.1,$$

$$\eta > 0, \qquad 1.1 \leqslant r \leqslant 2.2.$$

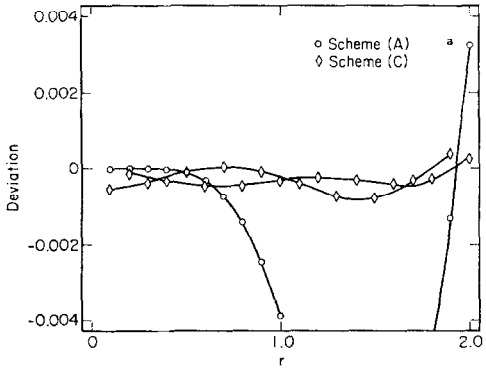

FIG. 6a. Deviations in $B(r)$ from the exact function for $E = +1$.

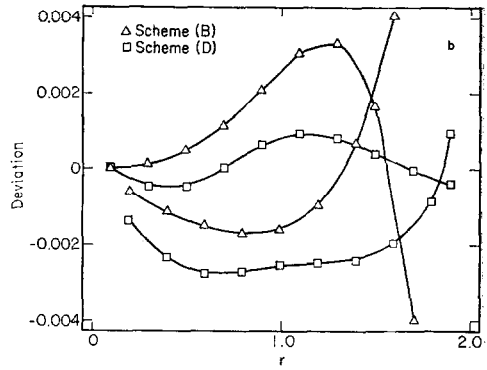

FIG. 6b. Deviations in $B(r)$ from the exact function for $E = +1$. Those for scheme (B) are 10 times larger than indicated.

The value 1.1 is remarkably accurate for predicting the positions of maximal error in (A), (B), and (D), while (38) and (39) also predict the monotonic growth and decay for (A) and the oscillations for (B) and (D). An extremely intriguing correlation for (C) is that, although the source of behavior is unknown, the intertwining of the even and odd errors occurs with very nearly the 1.1 wavelength!

We have made similar observations for smaller step sizes, and the results are predictable by (48) and (49). For smaller h, the deviations and oscillations are considerably less, but maintain the same qualitative behavior.

Recall that the more detailed error analysis did not evince the interesting behaviors just discussed, and was excused from doing so by faulting the assumption of constant $\mathbf{M}$. For the square well, $\mathbf{M}$ is about as slowly varying as it ever will be. Yet, for $E = -3$, the vector $\mathbf{W}(r)$ rotates about 90° between $r = 0$ and $r = 1$. Between $r = 1$ and $r = 2$, it maintains this perpendicular orientation, but grows by a factor of 10^3. For positive energies, $\mathbf{W}$ always has a constant length ($\mathbf{W} \cdot \mathbf{W} = k^{-1}$) and rotates with angle kr. When $E = 1$, this amounts to ~80° for each unit of r. Fortunately, it appears that the error analysis in (38) and (39) provides a reasonable framework for interpreting quadrature errors, and more exact results seem unnecessary.

We have performed calculations on several other potentials, since the square well is rather special and atypical of the problems usually encountered. One such was the Lennard–Jones potential

$$V = 108\,(r^{-12} - r^{-6}) \text{ Rydbergs.} \tag{50}$$

The phase shifts $\delta^{(1)}$ and $\delta^{(2)}$ for $E = 10$ and 100 were obtained for several h, as was the lowest eigenvalue $E^{(1)}$. For actual calculation, V was given an infinite hard

core at $r_0 = 0.5$, since $V(0.5) \sim 4 \times 10^5$. In Appendix C, we discuss two distinct methods of including this modification. The range of integration extended to 5.5 for the eigenvalue determination, and to 10.5 for the phase shifts. These values are not meant to give results converged in all respects to those of the exact potential, but the specified integration does provide a well-defined problem on which the performance of the various schemes can be compared. Tables VI–VIII contain the results. A most noteworthy feature appears in Table VII. For $E = 100$, a step size of 0.1 only puts $4\frac{1}{2}$ steps into each full wavelength of the wavefunction; schemes (C) and (D) are in error by $\sim 50\%$, yet scheme (A) gets δ to within 18%! Going to small h as described in Section 6, we can obtain the $h = 0$ results shown

TABLE VI

Lennard–Jones Phase Shift for $E = 10$, Calculated by Each Scheme for Several Step Sizes[a]

h	(A)	(B)	(C)	(D)
0.1	0.6048221883	0.5156067274	0.5737187323	0.6334273823
0.05	0.5776768849	0.5455550075	0.5711208047	0.5669223504
0.025	0.5711954818	0.5646763935	0.5691939037	0.5690242878
0.0125	0.5695927474	0.5679872240	0.5690685289	0.5690578854
0.00625	0.5691931418	0.5687933640	0.5690605646	0.5690599002
0*	0.5690585026	0.5690908342	0.5690600336	0.5690600345

[a] Row 0* results are extrapolated from $h = 0.00625$.

TABLE VII

Lennard–Jones Phase Shifts for $E = 100$, Calculated by Each Scheme for Several Step Sizes[a]

h	(A)	(B)	(C)	(D)
0.1	0.8581602679	1.553243597	1.065524863	1.098885110
0.05	0.7554347711	0.6566486675	0.7377628439	0.7192824489
0.025	0.7329784126	0.7108560024	0.7265172846	0.7255578619
0.0125	0.7275586097	0.7221558959	0.7258170590	0.7257558271
0.00625	0.7262151807	0.7248728283	0.7257714609	0.7257676109
0*	0.7257673710	0.7257784724	0.7257684210	0.7257683965

[a] Row 0* results are extrapolated from $h = 0.00625$.

TABLE VIII

First Lennard–Jones Eigenvalue, Calculated by Each Scheme for Several Step Sizes[a]

h	(A)	(B)	(C)	(D)
0.1	−3.659382251	—[b]	−3.510556783	−5.505594461
0.05	−3.539682107	−2.389180493	−3.506372090	−3.462707594
0.025	−3.511017559	−3.486912450	−3.501877859	−3.501465743
0.0125	−3.503925202	−3.496839632	−3.501587162	−3.501562600
0.00625	−3.502156660	−3.500388544	−3.501568778	−3.501567240
0*	−3.501527146	−3.501571515	−3.501567552	−3.501567549

[a] Row 0* results are extrapolated from $h = 0.00625$.
[b] Did not converge to any value.

TABLE IX

Summary of Efficiency Parameters from the Calculations on the Lennard–Jones Potential

		(A)	(B)	(C)	(D)
$\delta^{(1)}$	h_s	0.013	0.009	0.036	0.050
	$10^3\theta_s$	2.15	1.52	2.75	4.58
$\delta^{(2)}$	h_s	0.008	0.006	0.025	0.034
	$10^3\theta_s$	1.33	0.93	1.89	3.13
$E^{(1)}$	h_s	0.015	0.011	0.046	0.064
	$10^3\theta_s$	2.54	1.79	3.51	5.86

in the last row of each table, and use these values to compute and plot the percent deviations in the calculated values of E and δ as before. The h_s and θ_s values so obtained are listed in Table IX.

We make two observations. First, we have $\theta_A > \theta_B$ and $\theta_C < \theta_D$ for all three calculations. The reversal of the second inequality from the square well problems is curious. Second, and equally curious, we now have $h_D \sim 4h_C/3$ for each calculation. Apparently, scheme (D) works better than (C) on this potential.

For this problem, too, we have examined the numerical A and B functions and find, as before, that significant oscillations can develop in the results of (D) if h is not small enough. For example, integration with $h = 0.05$ for $E = -3.5$ gives a $B(r)$ which goes through a maximum of 0.2282(10) at step 10, becomes irregular

between steps 20 and 30 as the values at even and odd quadrature points begin to split apart, and finally shows the following oscillations for steps 40 through 43:

$$+0.4640(7), \quad -0.4618(7), \quad +0.4629(7), \quad -0.4643(7).$$

(Numbers in parentheses here are powers of 10.) These oscillations persist, even as the integrals "converge" beyond the range of V. By step 70, the function A behaves similarly. Redoing the integration with $h = 0.025$ produces a $B(r)$ which goes through a maximum of 0.9265(14) at step 20, again develops irregularities, and finally stabilizes with much less noticeable oscillations at steps 120 through 123:

$$-0.7486(10), \quad -0.7699(10), \quad -0.7482(10), \quad -0.7696(10).$$

For $h = 0.05$ and $E = 100$ (approximately 12 steps per wavelength of ϕ) the relative oscillations of $B(r)$ at step 40 are approximately 0.016.

The existence of such distinct values of the converged integrals at consecutive quadrature points might be expected to lead to distinctly different values of E or δ depending on whether the chosen integration range (r_0 to $r_0 + Nh$) contains an even or odd number of steps. In Table X, we compare schemes (C) and (D) for several different step sizes to see how much their calculated $\delta^{(1)}$, $\delta^{(2)}$, and $E^{(1)}$ differ if one stops the integration at step N or $N - 1$. Since quadrature errors in (A) and

TABLE X

Comparison of Schemes (C) and (D) at the Last Odd and Even Quadrature Points for the Calculations in Tables VI and VII

		(C)		(D)	
	h	Odd	Even	Odd	Even
$\delta^{(1)}$	0.1	0.573719	0.573719	0.468364	0.633427
	0.05	0.571121	0.571121	0.569934	0.566922
	0.025	0.569194	0.569194	0.569025	0.569024
$\delta^{(2)}$	0.1	1.065524	1.065525	0.330773	1.098885
	0.05	0.737763	0.737763	0.723080	0.719282
	0.025	0.726517	0.726517	0.725553	0.725558
$E^{(1)}$	0.1	−3.510557	−3.510557	—[a]	−5.505594
	0.05	−3.506372	−3.506372	−3.537734	−3.462708
	0.025	−3.501878	−3.501878	−3.501508	−3.501466

[a] Did not converge to any value.

(C) have previously appeared to be simple, smooth functions of r, we expect them to show little effect in this comparison. The errors for (B) and (D) oscillate, however, and may lead to significant differences between values at consecutive quadrature points. A small discrepancy is expected for all schemes since $V(r_0 + Nh)$ is not zero, though it is very nearly so. This slight effect is presumably the only cause of discrepancies for $h \leqslant 0.025$. However, for larger h, the discrepancies in scheme (D) results are too large to be accounted for thusly. Rather, these cases are those for which significant oscillations are occurring. For $h = 0.05$, the actual deviations in the integrals $\{A, B\}$ at consecutive quadrature points were approximately $\{0.6\,\%, 0.1\,\%\}$ and $\{0.8\,\%, 1.6\,\%\}$ during calculations for $\delta^{(1)}$ and $\delta^{(2)}$, respectively. However, the deviations in the δ values themselves were both $0.5\,\%$. This indicates that the oscillations in A and B maintain some phase coherence, thus moderating the overall error. The discrepancy in $E^{(1)}$ is about $2\,\%$ for this step size. The reason it is no worse is that the B integral whose magnitude is being forced to zero, can be forced as well from below as from above zero. Note that the magnitude 10^7 is "small" compared to the maximum B magnitude during the calculation.

We remark that both the A and B integrals computed by schemes (A), (B), and (D) get fairly large [14] for problems of this nature ($V(r_0)$ very large) since the first numerical contributions to B go as $hV(r_0)$, and those to A go as $h^2V(r_0)$. However, scheme (C) is not a step-by-step integration (it is implicit at odd quadrature points), so it does not give such artifically strong contributions for a given h, and for this problem it results in integral values of only half as many orders of magnitude. It may be useful to employ such implicit schemes always at the start of the integrations, but we have not pursued this.

Finally, we remark that comparisons similar to the above have been made for calculations on several other problems, e.g., bound states in the hydrogen p-state (Fues) potential $2/r^2 - 2/r$, scattering from the repulsive angular momentum barrier $l(l+1)/r^2$, and two different potentials which support shape resonance. All studies resulted in similar conclusions.

6. Generalized Richardson Extrapolation

"Richardson extrapolation," or "Richardson's deferred approach to the limit," is a method which attemtps to eliminate the dependence of a numerically determined integral on the quadrature scheme used for its evaluation [15]. We have previously applied this idea to the noniterative integral equation method for determination of R-matrix elements for $h = 0$ in a multichannel $e - H$ scattering calculation and found it to be remarkably accurate [16]. Our "generalization" is to apply the idea to E and δ directly, rather than to the integrals used for their determination. We now apply it to the schemes investigated here.

Referring to Figs. 1–4, the linearity of the log–log plots suggests that the calculated quantities $q_s(h)$ have a well-defined step size dependence in the form

$$q_s(h) = q(0) + \alpha_s h^{\gamma_s}, \tag{51}$$

as long as h is not too large. Heuristically, such a form can be argued as follows. The quadrature formulas we have used are related to exact integration by error terms of the form $Nh^n[d^n\mathbf{P}/dr^n]_{r=\xi}$, where ξ lies within the interval of integration $L = Nh$. Suppose that ξ does not change much as h is reduced. (The conditions under which this is true for the trapezoidal rule were studied by Richardson and Gaunt [17].) Then not only do we have a bound on the quadrature error, but we expect it to depend on h approximately as cLh^{n-1}. Since $q_s(h)$ depends in a simple algebraic manner on the calculated integrals, this leads to (51) with γ_s one less than the order of local truncation for the quadrature scheme. To be generally useful, we should like γ to depend only on the scheme and not the problem at hand, although α should depend on both. We now summarize the relevant consequences of assuming (51), and then apply them to the calculations in Section 5.

We can calculate γ_s easily from (51) if we have q_s at three values of h. Specifically, given $q_s(h)$, $q_s(2h)$, and $q_s(4h)$, we eliminate $q(0)$ and αh^{γ} to get

$$\gamma_s = (\ln 2)^{-1} \ln \left[\frac{q_s(2h) - q_s(4h)}{q_s(h) - q_s(2h)}\right]. \tag{52}$$

Furthermore, we can eliminate αh^{γ} from (51) written for $q_s(h)$ and $q_s(2h)$ to arrive at a simple extrapolation law

$$q(0) = q_s(h) + (2^{\gamma_s} - 1)^{-1} [q_s(h) - q_s(2h)], \tag{53}$$

giving the exact value of q in terms of calculated quantities. Let t be the specified tolerance allowed in q_s. This is achieved if h is less than the value h_s determined from

$$t = |[q_s(h_s) - q(0)]/q(0)|. \tag{54}$$

This gives h_s as

$$h_s = | \, tq(0)/\alpha_s \, |^{1/\gamma_s}, \tag{55}$$

where α_s comes from

$$\alpha_s = [q_s(2h) - q_s(h)]/h^{\gamma_s}(2^{\gamma_s} - 1). \tag{56}$$

These equations provide the method by which the results in Tables V and IX were actually obtained.

TABLE XI

Values of the Generalized Richardson Exponent γ_s, Calculated from the Square Well and Lennard–Jones Potential Results[a]

	(A)	(B)	(C)	(D)
Square well				
$E^{(1)}$	2.0024	2.8581	3.9979	2.9303
$E^{(2)}$	2.0029	2.7297	4.0049	2.9833
$\delta^{(1)}$	2.0074	2.8972	4.0021	3.2097
$\delta^{(2)}$	2.0062	1.7455	3.9891	2.9933
$\bar{\gamma}$	2.0047	2.5576	3.9985	3.0292
	(0.12%)	(21.%)	(0.17%)	(4.1%)
Lennard–Jones				
$\delta^{(1)}$	2.0039	2.0381	3.9766	4.0596
$\delta^{(2)}$	2.0123	2.0563	3.9408	4.0704
$E^{(1)}$	2.0037	1.4840	3.9830	4.3836
$\bar{\gamma}$	2.0066	1.8595	3.9668	4.1704
	(0.24%)	(17.%)	(0.57%)	(4.4%)

[a] The average exponent $\bar{\gamma}$ for each scheme is computed for each potential; its percentage standard deviation is in parentheses.

The discussion following (51) suggests that the values of γ_s should be $\gamma_A = \gamma_B = 2$ and $\gamma_C = \gamma_D = 4$. To see if these were correct, we applied (52) to the data in Tables I–IV, taking $h = 0.025$, and to the data in Tables VI–VIII, taking $h = 0.00625$. The two sets of γ_s so obtained are shown in Table XI.

The calculated average values $\bar{\gamma}_s$ from the square well results would lead to integral exponent choices $\gamma_A = 2$, γ_B indeterminate, $\gamma_C = 4$, and $\gamma_D = 3$, while the Lennard–Jones averages suggest $\gamma_A = \gamma_B = 2$, and $\gamma_C = \gamma_D = 4$. From the percent standard deviations given in parentheses, we must reject the use of Richardson extrapolation for (B). We are also discouraged by the apparent dependence of γ_D (as well as γ_B) on the problem being solved. These two schemes were also the only ones to show obvious deviations from linearity in Figs. 1–4. The conclusion here is that (51), with γ determined from the error term for the scheme, is not suitable for "overlapping" schemes, but can be expected to be reliable for repeated segmental schemes like (A) and (C).

To demonstrate the validity and usefulness of the extrapolation law in (53), we used the assumed exponents $\gamma_A = \gamma_B = 2$, $\gamma_C = \gamma_D = 4$, and applied it to the data in Tables I–IV and VI–VIII. In the square well problem, we used $h = 0.0125$

to get the first set of values for $h = 0$ (labeled 0^*) and then repeated the extrapolation from further out, $h = 0.025$ (labeled 0^+). As expected, for (A) and (C) the extrapolation is very good, and picks up several orders of magnitude closer agreement with the exact results.

In the Lennard–Jones problem, we took $h = 0.00625$ for the extrapolation. Both (C) and (D) show excellent agreement (recall $\bar{\gamma}_D$ here was close to the assumed value of 4) and we assume their average extrapolants to be the correct zero step size result. This gives the values of $q(0)$ used in (55) and (56) for evaluating h_s and θ_s for this problem in Table IX.

Our generalized Richardson extrapolation (applied to $q_s(h)$, rather than to the integrals themselves) has two primary uses. First, calculated results can be converted into quadrature-independent values, as we have done here. Second, it can be applied in reverse to estimate quadrature error in results calculated with finite step size h. As an example, one can calculate δ for a number of step sizes to determine that h is actually in the region for which (51) holds. Then $|[\delta(h) - \delta(2h)/(2^{\gamma_s} - 1)\,\delta(h)]|$ gives an estimate of the quadrature error present in the calculation with step size h. For problems as complex as $e - H$ scattering, such estimates are found to be relatively insensitive to E, although they do differ for different partial wave sets. Thus, one obtains quite easily a quantitative statement of convergence of his results with respect to h. Quantities of kinetic interest can then be computed, with their quadrature-related error approximately known.

Conclusions

We have shown that for the noniterative integral equation method the quadratic schemes (C) and (D) are generally superior to the linear schemes (A) and (B) in both accuracy and efficiency, with little additional storage requirements. This is in accord with earlier studies [3]. Scheme (B) was found to serve no useful purpose in this application. Scheme (A) has demonstrated well its most attractive features—simplicity of implementation, stability of solution, and extremely accurate correction to zero step size by an h^2 Richardson extrapolation.

For specified accuracy, scheme (C) allows at least a threefold increase in step size for all cases considered [18]. Scheme (D) allows a twofold increase in the square well problem, and a fourfold increase in the Lennard–Jones case. This is enough to make both more efficient in execution than (A), and to reduce significantly the number of required f, g, and V evaluations. Both have similar storage requirements, and nearly the same number of operations per step. However, we have found that scheme (D) has a disturbing tendency toward instability, which must be checked carefully for each application. Oscillations between even and odd quadrature points, which may not be large enough to cause obvious errors in an

unfamiliar problem, can affect the results by several percent. These oscillations appear to be inherent in the overlapped nature of the scheme, and can only be controlled by step size reduction. This problem has not received much attention, presumably because the scheme has been mostly used in scattering problems where the effect is smaller. Bound state problem bring out the worst in the scheme, so it seems unsuitable for these. This may be of concern for the closed channels in a close coupled computation and is currently being investigated. Finally, we found that Richardson extrapolation is not reliable here, since γ depends on the problem and may or may not be the expected value 4. Of course, an appropriate γ can be found, but this requires additional study of each problem.

Scheme (C), our quadratic rule, seems to be free of such difficulties. It appears to be essentially as stable as (A) for any h, which was suggested by the error analysis. This was even enhanced for bound state problems, contrary to (D). The only oscillation which was found had very small magnitude (see Fig. 6a), and was due to the oscillation of the propagation matrix $\mathbf{M}$ itself. Finally, (C) was found to allow very accurate Richardson extrapolation with the assumed exponent $\gamma = 4$, independent of the problem.

An interesting scheme [19] which we have not studied consists in cyclic use of the ordinary Simpsons rule in (20) with Simpson's "3/8 rule,"

$$\mathbf{P}_{n+3} = \mathbf{P}_n + (3h/8)(\mathbf{P}_n' + 3\mathbf{P}'_{n+1} + 3\mathbf{P}'_{n+2} + \mathbf{P}'_{n+3})$$

with error $-3h^5\mathbf{P}^{(5)}/80$. Given $\mathbf{P}_n$ and $\mathbf{P}_{n+1}$, one uses (20) to get $\mathbf{P}_{n+2}$, then uses these three values in the "$\frac{3}{8}$ rule" to get $\mathbf{P}_{n+3}$. The cycle is then repeated, starting with $\mathbf{P}_{n+2}$ and $\mathbf{P}_{n+3}$ and obtaining successively $\mathbf{P}_{n+4}$ and $\mathbf{P}_{n+5}$. Similar to our quadratic rule, both calculated points are apparently constrained to lie on the same approximating cubic and are not expected to lead to the instability which offends the overlapped Simpson's rule.

Appendix A

In abbreviated notation, we rewrite (1) as

$$\psi = \gamma f + g\int_0^r fV\psi\, dr + f\int_r^\infty gV\psi\, dr, \tag{A1}$$

where $\gamma = 0$ or 1. We then use $\int_r^\infty dr = \int_0^\infty dr - \int_0^r dr$ to get

$$\psi = g\int_0^r fV\psi\, dr + f\left(I - \int_0^r gV\psi\, dr\right), \tag{A2}$$

where $\Gamma = \gamma + \int_0^\infty f V\psi \, dr$, and is an unknown constant. Assuming it is nonzero, introduce a new function by $\psi(r) = \phi(r)\,\Gamma$. Then Γ factors from (A2) to give (2) of the text, with Γ defined by

$$\left(1 - \int_0^\infty gV\phi \, dr\right)\Gamma = \gamma. \tag{A3}$$

Since Γ is [illegible] required asymptotic form of ψ also demands that $1 - \int_0 gV\phi \, dr = 0$, thus leaving Γ completely arbitrary.

Appendix B

Inasmuch as the square well potential provides an undergraduate problem in quantum mechanics, we only summarize the necessary results not usually given in textbooks. The two wavenumbers of importance are the one in the well ($0 \leqslant r \leqslant a$)

$$H = (-V + 2E)^{1/2}, \qquad V \text{ in units of } 2E,$$

and the one in the zero-potential region ($r > a$)

$$K = |\, 2E \,|^{1/2}.$$

These expressions are valid for both $E < 0$ and $E > 0$. For $E < 0$, the function B is

$$B(r) = e^{-Kr}(\cos Hr + K \sin Hr/H). \tag{B1}$$

Eigenvalues are those values of E for which $B(a) = 0$, and the well-known transcendental equation for such values follows from (B1). For $E > 0$, the function is

$$B(r) = (2H)^{-1}\,[(H + K)\cos(H - K)\,r + (H - K)\sin(H + K)\,r], \tag{B2}$$

with the phase shift beyond $r = a$ given by

$$\tan\delta = \frac{K \cot aK - H \cot aH}{K + H \cot aH \cot aK}. \tag{B3}$$

As mentioned in the text, the availability of these analytical results, especially $A(r)$ and $B(r)$ for arbitrary $E < 0$, makes this problem quite important for the testing of numerical schemes.

APPENDIX C

We briefly show the equivalence of two approaches in the integral equation method for introducing a hard core at r_0 to simulate the effect of potentials which are extremely large at separations less than r_0.

In the first approach, one means by "hard core boundary condition" that the actual potential in the interval $[0, r_0]$ is so large that the wavefunction $\phi(r_0)$ is still essentially zero for numerical purposes. From (2), this suggests that the initial condition in (4) be modified to

$$P(r_0) = c \begin{pmatrix} f(r_0) \\ -g(r_0) \end{pmatrix}. \tag{C1}$$

and integration performed from r_0 into the asymptotic region to obtain the phase shift δ. The absolute magnitudes of $A(r_0)$ and $B(r_0)$ are arbitrary, so c can be chosen small enough that propagation from r_0 out to the classical region does not lead to unreasonably large integrals. We note that if V is zero for $r > r_0$, then one correctly obtains the "hard sphere" phase shifts

$$\delta_0 = \tan^{-1}(f(r_0)/g(r_0)). \tag{C2}$$

Thus, this procedure inserts the hard core phase shift into the boundary conditions of the integration.

An alternative view of the "hard core boundary condition" is that the wavefunction is rigorously zero in $[0, r_0]$. In the theory of Green's functions, the inner and outer solutions are constructed to satisfy the boundary conditions of the problem, so r_0 becomes the effective origin, and in terms of the variable $\rho = r - r_0$ we take (e.g., for $l = 0$)

$$f(\rho) = k^{-1/2} \sin k\rho, \qquad g(\rho) = -k^{-1/2} \cos k\rho. \tag{C3}$$

We then compute the solution to (4) in terms of ρ, but with $V(\rho + r_0)$ appearing instead of $V(r)$. Obviously, the phase shift $\tilde{\delta}$ calculated by this procedure is relative to the origin at r_0, so one has to add the "hard sphere" phase shift to get the correct result

$$\delta = \tilde{\delta} + \delta_0. \tag{C4}$$

For s-wave scattering, we find from (C2) and (45) that δ_0 is just kr_0, for example.

We favor neither method over the other for this simple problem, the only distinction being whether δ_0 is put in at the beginning or end of the calculation. However, the first method is probably to be preferred in the multichannel case,

since the second method would require a rephasing of both the A and B matrices before calculation of the R matrix.

With respect to bound state eigenvalue determinations, the meaning of "hard core boundary condition" is irrelevant. Eigenvalues are intrinsic to the *shape* and *magnitude* of the specific potential, but not to its *location*. They will therefore be identical regardless of the method used to handle the hard core. Phase shifts, on the other hand, depend explicitly on the choice of origin by virtue of their definition as the phase of a scattered wave relative to a free wave emanating from the origin.

ACKNOWLEDGMENTS

The author wishes to thank Professors W. H. Miller and H. F. Schaefer for their hospitality during his stay at Berkeley, and is pleased to acknowledge Professor Keith Miller for several helpful discussions concerning the error propagation. Valuable discussions with Professor E. F. Hayes and Dr. Lee Collins concerning the hard core modification are gratefully acknowledged. The computations necessary for this study were made on the Harris Corporation Slash Four minicomputer, which is supported by the National Science Foundation under GP-39317. This study was supported by the Miller Institute for Basic Research in Science at the University of California.

REFERENCES

1. W. N. SAMS AND D. J. JOURI, *J. Chem. Phys.* **51** (1969), 4809; *J. Chem. Phys.* **51** (1969), 4815.
2. W. N. SAMS AND D. J. KOURI, *J. Chem. Phys.* **52** (1970), 4144; *J. Chem. Phys.* **53** (1970), 496; D. J. KOURI, *J. Chem. Phys.* **51** (1969), 5204; W. G. COOPER AND D. J. KOURI, *J. Chem. Phys.* **57** (1972), 2487; D. L. KNIRK, E. F. HAYES, AND D. J. KOURI, *J. Chem. Phys.* **57** (1972), 4770; R. A. WHITE AND E. F. HAYES, *J. Chem. Phys.* **57** (1972), 2985, *Chem. Phys. Lett.* **14** (1972), 98; E. R. SMITH AND R. J. W. HENRY, *Phys. Rev.* **A7** (1973), 1585, *Phys. Rev.* **A8** (1973), 572.
3. E. F. HAYES AND D. J. KOURI, *J. Chem. Phys.* **54** (1971), 878; D. SECREST, *Methods Comput. Phys.* **10** (1971), 274.
4. These equations are similar to the auxillary $T^{(k,j)}$ matrix equations of Hayes and Kouri [3], but use a different boundary condition to obtain a simpler form.
5. An exact solution of such differential equations is available in the matricant series [see F. R. GANTMACHER, "The Theory of Matrices," Chelsea, New York, 1964)]. This is just the infinite-order Born series for the scattering problem. An approximate solution from some point r_N to infinity has been discussed by Knirk [D. L. KNIRK, *J. Chem. Phys.* **57** (1972), 4782; K. OMIDVAR, *Phys. Rev.* **A 133** (1964), 970; see also Smith and Henry [2]] and leads to a natural technique within the noniterative integral equation method for including simply the effects of long-range potentials.
6. W. E. MILNE, "Numerical Solution of Differential Equations," Dover, New York, 1970.
7. [6, p. 42].
8. Called "Method I" in [6, p. 19].
9. The basic idea, which is not new, is the basis for the implicit Runge–Kutta schemes described by J. D. BUTCHER, *Math. Comput.* **18** (1964), 50.

10. [6, Eq. (19.1) and (19.2), p. 48].
11. A. RALSTON, "A First Course in Numerical Analysis," pp. 161–179, McGraw–Hill, New York, 1965.
12. Cf. [6, pp. 29–30].
13. Cf. [6, pp. 22–23].
14. Of course, since $\mathbf{P}(r)$ depends linearly on $\mathbf{P}(r_0)$, the numerical results may always be scaled down to convenient values by simply scaling $\mathbf{P}(r_0)$. See Appendix C.
15. See, for example [11, pp. 118–121].
16. D. L. KNIRK, Ph. D. Dissertation, pp. 256–266, Rice University, 1972.
17. L. F. RICHARDSON AND J. A. GAUNT, *Trans. Roy. Soc. London* **A 226** (1927), 299.
18. We certainly did not get the tenfold increase claimed by Hayes and Kouri [3], but their study was made on a multichannel problem.
19. E. F. HAYES, private communication.